Proposal to Jefferson Lab PAC 24

Pion Photoproduction from a Polarized Target

R. A. Arndt, N. Benmouna[1], C. Bennhold, B. L. Berman, W. J. Briscoe, G. Feldman, Y. Ilieva, H. Juengst, F. Lee, I. I. Strakovsky[1], S. Strauch[1,*], R. L. Workman
The George Washington University, Washington, DC 20052

G. V. O'Rielly[1]
University of Massachusetts Dartmouth, MA 02747

J. Ball, M. Dugger, E. Pasyuk, B. G. Ritchie
Arizona State University, Tempe, AZ 85287-1504

H. Crannell, F. J. Klein, D. I. Sober
The Catholic University of America, Washington, DC 20064

R. Schumacher, L. Todor
Carnegie Mellon University, Pittsburgh, PA 15213

V. Kouznetsov
Institute for Nuclear Research, 117312, Moscow, Russia

D. M. Manley
Kent State University Kent, OH 44242

V. Mokeev
Moscow State University, 119899 Moscow, Russia, and Jefferson Lab

M. Khandaker
Norfolk State University, Norfolk, VA 23504

R. Gilman
Rutgers Univserity, Piscataway, NJ 08854

V. Burkert, H. Egiyan, L. Elouadrhiri, B. Mecking, Y. Sharabian, S. Stepanyan, U. Thoma, B. B. Wojtsekhowski
Thomas Jefferson National Accelerator Facility, Newport News, VA 23606

M. F. Vineyard
Union College, Schenectady, NY 12308

C. Djalali, O. Dzyubak, D. Tedeschi, M. Wood
University of South Carolina, Columbia, SC 29208

P. L. Cole
University of Texas at El Paso, El Paso, TX 79968

D. G. Crabb
University of Virginia, Charlottesville, VA 22901

D. Jenkins
Virginia Polytechnic Institute and State University, Blacksburg, VA 24061

and the CLAS Collaboration

[1] Co-spokesperson
[*] Contact person

Abstract

We propose to study single-pion photoproduction reactions, $p(\gamma, \pi^+)n$ and $p(\gamma, p)\pi^0$, with polarized beam and longitudinally as well as transversely polarized target using the CLAS detector at Jefferson Lab Hall B. The experiment will measure two single- (T and P) and three double-polarization observables (G, F, and H); experiment E01-104 will measure the double-polarization observable E. The data will greatly constrain partial-wave analyses and reduce model-dependent uncertainties in the extraction of nucleon resonance properties, providing a new benchmark for comparisons with QCD-inspired models. The measurement will span $\cos(\theta_{cm})$ from -0.9 to 0.9 in a center-of-mass energy range above 1300 MeV and up to 2150 MeV.

1 Introduction

The nature of QCD confinement continues to provide an ongoing challenge to our understanding of soft QCD. Studying the baryon spectrum provides one avenue to learn more about this unique feature since the location and properties of excited states reflect the dynamics and relevant degrees-of-freedom within hadrons.

Through analyses of decades worth of data, from both hadronic and electromagnetic scattering experiments, we have found numerous baryon resonances, and have determined their masses, widths, and quantum numbers. Many more states have been predicted by quark models. If they exist, these states have either eluded detection or have produced only weak signals in the existing data sets. The search for such resonances provides a natural motivation for future measurements at Jefferson Lab.

A more complete knowledge of the resonance spectrum would be invaluable to studies that aim to elucidate the detailed dynamics and degrees-of-freedom responsible for the baryon spectrum. These include QCD lattice calculations, various constituent quark models, QCD sum rules, and unitary ChPT. For example, there is the interesting possibility of chiral-symmetry restoration exhibited by the high-lying (and poorly determined) states [1]. It is equally important to have precisely determined properties for the well-established resonances, as these are likely to be less model-dependent, and existing data already suggest deviations from constituent-quark-model predictions for their decay properties [2].

While a few resonances (such as the $\Delta(1232)$, $N(1520)$, and $N(1680)$) have a strong signal in the cross section, with clear Breit-Wigner behavior in their associated multipole amplitudes, these are exceptional cases. In general, more detailed analyses of the experimental data are required to extract properties of the N^* and Δ^* resonances. As we will demonstrate, data sets restricted to unpolarized cross sections and single polarization observables alone are not sufficient to resolve discrepancies between the extensive SAID [3] and MAID [4] analyses. The need for the measurement of double polarization observables, which require a polarized target, then becomes obvious.

Pion photoproduction has long been analyzed in order to extract the photo-decay amplitudes associated with the N^* and Δ^* resonances. Extensive fits to elastic pion-nucleon scattering have provided mass and width values for the contributing resonances. Multipole phases are also linked to corresponding pion-nucleon phase shifts, through Watson's theorem, up to the onset of inelasticity (2π production).

However, above the two-pion production threshold, multipole analysis becomes increasingly model-dependent. The GW Data Analysis Center (SAID) and Mainz (MAID) fits to this region attempt to describe the available data, within the constraints obtained from pion-nucleon scattering from the SAID analysis [5], employing different phenomenology. In the MAID approach, resonance parameters are varied in fitting the data. The SAID approach is to first obtain multipole amplitudes in a manner that is as "model-independent" as possible. The extracted multipoles are then refitted to functional forms having both resonance and background contributions.

Differences between these approaches are most evident in predictions for observables not yet measured. Each new measurement provides further constraints related to a different bi-linear combination of helicity amplitudes. Below, we outline what types of data are currently available in the database, and consider which measurements are both necessary and best suited to the CLAS detector.

The CLAS detector, with its ability to measure both θ and ϕ distributions over a broad angular range, combined with the Photon Tagging Facility in Hall B at Jefferson Lab, is uniquely positioned to host a new generation of high-quality photoproduction experiments, with small statistical errors and well understood systematic uncertainties. An example of pion photoproduction with an unpolarized target is given in Ref. [6]. The availability of linearly polarized photons and an unpolarized target enables the measurement of differential cross sections and beam asymmetry Σ, only. At present, data for $d\sigma/d\Omega$ have been taken during the g1 run period, and data for Σ were taken during the g8a run period with CLAS. The full potential of CLAS will be achieved with the addition of a polarized target.

2 Motivation

2.1 Scope of the Proposed Program

A comparison of recent coupled-channels analyses [7] comes to the conclusion that, for most cases, it is only the first excited state in each partial wave whose detailed properties (partial branching fractions, helicity amplitudes) are well known. Different analyses may agree on the existence of the second state (in each partial wave) but not on their decay properties, while there is no agreement even on the existence of a third state in a particular partial wave. Given the arduous nature of the task involved in obtaining high-quality data that enter these multichannel analyses it is reasonable to address the question as to the final scope of this effort. In other words: How many resonances do we need to identify in order to convince ourselves that we have achieved a solid understanding of the baryon spectrum from QCD? As examples, we examine this question from the viewpoint of lattice gauge and constituent quark model calculations.

Recent lattice calculations suggest that Euclidean-space Monte Carlo calculations can reliably extract the properties of excited states. For example, using the constrained-fitting method based on Bayesian priors, ref. [8] extracts the masses of the two lowest-lying states of octet and decuplet baryons for both parities. The calculation, using an improved gauge action and overlap fermions with a pion mass as low as 180 MeV, clearly observed the $1/2^{+}(1440)$ Roper state for the first time as the first excited state of the nucleon from the standard interpolating field. Using correlator matrix techniques with a suitable number of reasonably well chosen operators, lattice simulations can indeed reveal information about higher-lying states in a given symmetry channel. The Lattice

Hadron Physics Collaboration (LHPC) centered at JLab and MIT is currently embarking on a large project to compute the N^* spectrum [18]. Given currently available computer resources and algorithms, it is likely that a reasonably accurate determination of a half-dozen states in several J^{PC} channels will be obtained in the quenched approximation for quark masses as light as 300 MeV in the next 1-2 years.

In the quark model approach the effective degrees-of-freedom are constituent quarks. Various QCD-based models disagree about the nature of the short-range, tensor and spin-orbit interactions between the quarks. There are now three competing models for the short-range interaction between light quarks in baryons: one-gluon exchange, instanton-induced forces, and Goldstone-boson exchange (recently supplemented by scalar- and vector-meson exchange). Given the present state of knowledge of the baryon spectrum, all of these models can explain the data to some degree of accuracy. If our knowledge of the baryon spectrum could be improved to perhaps half a dozen excited states in selected partial waves, along with detailed decay properties, a much clearer picture of the quark-quark interactions in baryons would emerge. In standard potential models such quarks are treated symmetrically, unlike those in quark-diquark and collective models. All symmetric quark models predict an overabundance of excited states relative to what has been observed until now: the well-known "missing" resonance problem. Diquark models predict fewer states by investing binding energy into a tightly bound isoscalar-scalar diquark which may push some positive-parity excitations higher in mass, leading to a deficit of positive-parity states at intermediate (1700-2000 MeV) energies. In addition to the as yet unidentified qqq states, confinement models using flux tubes predict the lightest qqq hybrid baryons with $P_{11}, P_{13}, P_{31}, P_{33}$, and F_{35} quantum numbers [9]. In addition, there are states such as the Roper resonance which are hard to explain as pure qqq excitations, and so may be mixed with hybrid baryons. All baryon hybrids have conventional quantum numbers, so if they are to be found, we need to find (as has now been convincingly done with the glueball and scalar-isoscalar mesons) a surplus of states above those required by qqq potential models, and extract their predicted anomalous decay properties. Thus, in order to establish the existence of hybrid baryons, coupled-channel analysis methods must be able to extract *all* qqq states in the energy range of about 1700-2200 MeV.

2.2 Observables

There are three particles in the reaction $\gamma N \to N\pi$ that can carry polarization: the photon, target nucleon, and recoil nucleon. Hence, there are three possible double-polarization experiments: beam/target, beam/recoil, and target/recoil. The total number of observables is 16, though not all are independent. The formalism and definitions of observables commonly used to describe pseudoscalar meson photoproduction can be found in Ref. [10]. Since one cannot easily measure recoil polarization with CLAS, we are left with the beam/target group, and we will discuss only these observables; they are given in Table 1.

The cross section for the beam/target polarization experiment is expressed

Table 1: Observables in single-pion photoproduction with polarized target and/or polarized photons. See also Ref. [10].

	Photon beam		
Target	unpolarized	circularly polarized	linearly polarized
unpolarized	$d\sigma/d\Omega$	—	Σ
longitudinally	—	E	G
transversely	T	F	H, P

as

$$\frac{d\sigma}{d\Omega} \bigg/ \frac{d\sigma}{d\Omega}_{\mathrm{unpol}} = 1 - P_T \Sigma \cos(2\varphi) \\ +P_X \left[-P_T H \sin(2\varphi) + P_\odot F\right] \\ -P_Y \left[-T + P_T P \cos(2\varphi)\right] \\ -P_Z \left[-P_T G \sin(2\varphi) + P_\odot E\right] \ , \quad (1)$$

for various orientations of the beam and target polarization. In the above expression, $P_\odot$ is the degree of right-circular beam polarization, P_T gives the transverse beam polarization (at an angle φ with respect to the reaction plane), and $P_{X,Y,Z}$ is the target polarization. A schematic of the reaction is shown in Figure 1. When Hall B is equipped with a polarized target, all observables from Table 1 will become measurable.

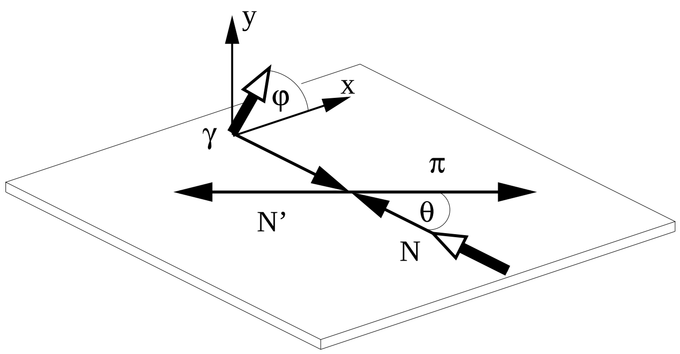

Figure 1: Schematic of the $\gamma N \to N\pi$ reaction in the center-of-mass frame; shown here with linearly polarized photons on a longitudinally polarized target.

Table 2: Relative weight of unpolarized and polarized data in the current database for pion photoproduction up to $E_\gamma = 2.0$ GeV.

Measurements	$p(\gamma, p)\pi^0$	$p(\gamma, \pi^+)n$
unpolarized	76%	70%
single-polarized	22%	27%
double-polarized	2%	3%

2.3 Previous Measurements

While a formally complete experiment requires the measurement, at each energy and angle, of at least eight observables [11], the current database for pion photoproduction is populated mainly by unpolarized cross sections. Table 2 illustrates this quite clearly.

Above the second resonance region (W=1520 MeV), the existing database for pion photoproduction is quite sparse, with few experiments covering large angular ranges at fixed energies. This shortcoming, coupled with the need to simultaneously analyze data from several laboratories (with different inherent systematic errors) often measured decades apart, has necessarily led to highly model-dependent analyses.

In 1994 [6], bremsstrahlung data comprised over 85% of the existing measurements. These data often suffered from significant uncertainties in normalization that were not completely understood or not quoted. The available tagged-photon data were generally low-statistics experiments, and hence were presented with large energy and angular binning. Much of the remaining data sets were comprised of excitation cross sections with no extensive angular range. Inconsistencies were obvious almost everywhere comparisons could be made. The full database has increased by 30% over the last eight years. The majority of these new data have come from tagged-photon facilities at MAMI (Mainz), GRAAL (Grenoble), and LEGS (Brookhaven.) The total database has doubled over the last two decades [3]. The distribution of available $\pi^0 p$ and $\pi^+ n$ data is given in Figures 2 and 3 (there are no new $\pi^- p$ and $\pi^0 n$ data, except for pion-capture data from TRIUMF.)

The number of data points from the proposed measurements are compared to available data, between 400 MeV and 2000 MeV in photon energy, in Table 3.

2.4 Phenomenology / Partial Wave Analysis

As is evident from Figure 4, cross section data alone are insufficient to isolate resonance contributions and distinguish between the various analyses. The resonance region may include on the order of 100 resonances, but has only two distinct "bumps" above the first resonance region.

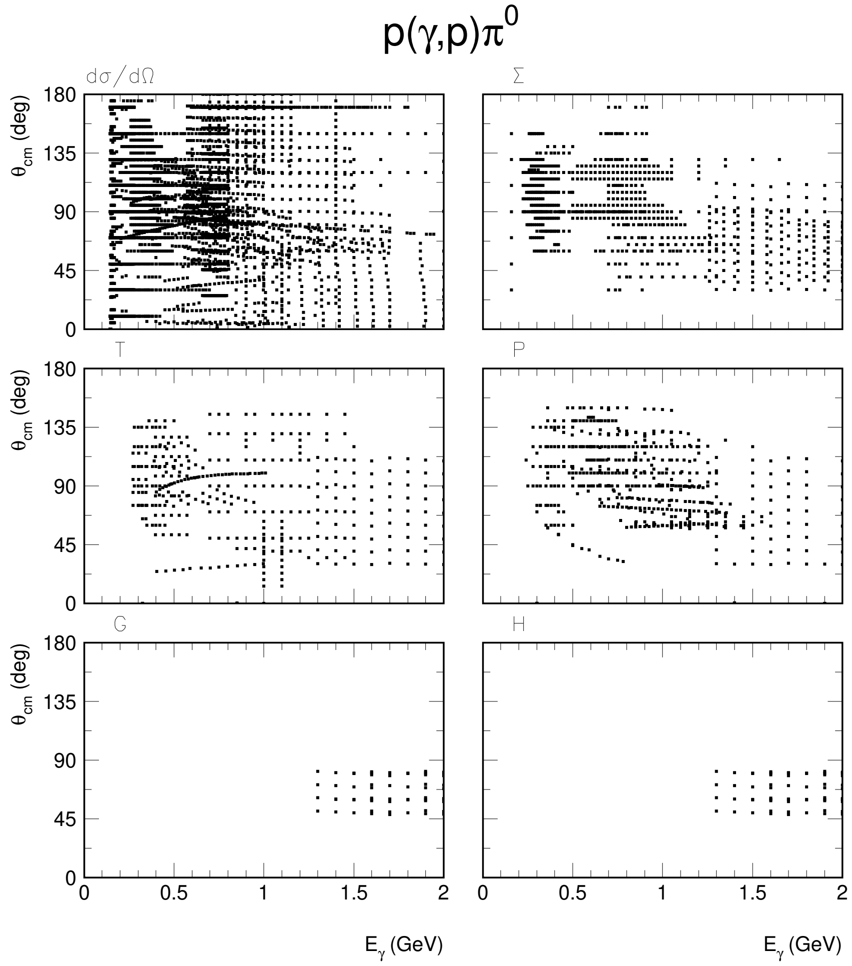

Figure 2: Available cross section and beam-target polarization measurements for the $\gamma p \rightarrow \pi^0 p$ reaction up to $E_\gamma = 2$ GeV. No data are available for the observables E and F.

The beam asymmetry, Σ, has been useful in separating resonance components from background in the $\Delta(1232)$ region, and more recently at higher energies [12]. Whereas both SAID and MAID analyses agree reasonably well for Σ (top part of Figure 5), there is a substantial difference in their predictions for G. This, perhaps, is not so surprising. Each polarization quantity involves a different bi-linear combination of helicity amplitudes. Even small changes in helicity amplitudes can result in very large changes for measurable quantities due to delicate interference effects.

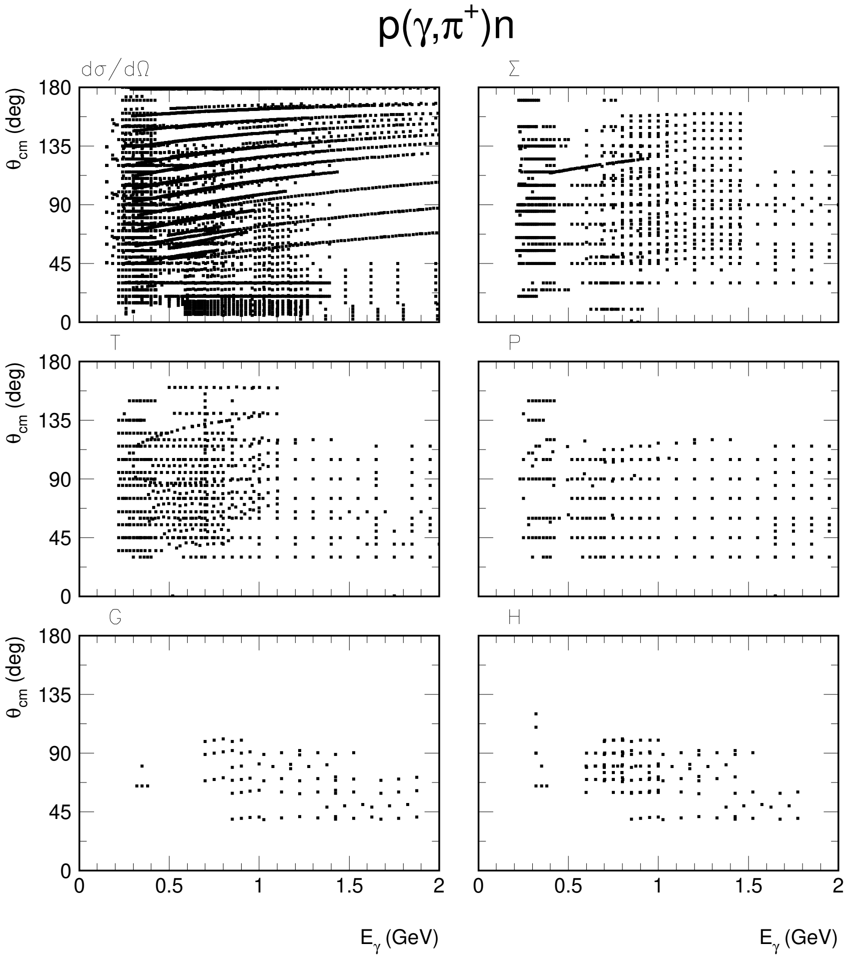

Figure 3: Available cross section and beam-target polarization measurements for the $\gamma p \to \pi^+ n$ reaction up to $E_\gamma = 2$ GeV. No data are available for the observables E and F.

The influence of double-polarization measurements was recently demonstrated through measurements of the beam-recoil quantities $C_{x'}$ and $C_{z'}$ in Hall A of Jefferson Lab [13]. While qualitative agreement with the existing SAID and MAID fits existed at lower energies, where comparisons could be made, the deviations at 1620 and 1900 MeV were much larger. In Figure 6, we compare SAID results (SM02) prior to the measurement of Ref. [13], including the new P_y, $C_{x'}$, and $C_{z'}$ points (SG02), and a forced fit (SC02). (The forced fit has increased the weight of the data of Ref. [13] by a factor of 4. By weighting

Table 3: Number of data points from available (two left columns) and proposed (two right columns) polarized beam and beam/target measurements, for photon energies $E_\gamma = 400$ MeV to 2000 MeV (where $DX13$ is the difference between the differential cross sections for pion photoproduction on the proton in the helicity-1/2 and helicity-3/2 states, $d\sigma/d\Omega_{1/2} - d\sigma/d\Omega_{3/2}$).

	Available data		Proposed data	
Observables	$p(\gamma,p)\pi^0$	$p(\gamma,\pi^+)n$	$p(\gamma,p)\pi^0$	$p(\gamma,\pi^+)n$
P	556	200	396	407
Σ	549	701	—	—
T	333	553	884	909
G	60	76	396	406
H	59	120	396	407
$E/DX13$	77	—	—	—
F	—	—	452	481

the data, we magnify changes in the multipole amplitudes, and more clearly see where data conflicts occur.) Except for a few points, the fit including data from Ref. [13] is not appreciably different from the "forced" fit, and appears to adequately describe these new results. However, a sharp structure at about 60° is seen in the forced fit. This is correlated with the improved fit seen for the target-polarization quantity T. This hints at the possibility of significant changes with the inclusion of precise new polarization data. A rapid angular variation is seen in both the polarization transfer and recoil polarization, showing the importance of measurements covering a wide angular range.

An overview comparison of SAID and MAID calculations for selected single- and double-polarization observables is shown in Figure 7. Plotted is the squared difference between the SAID and MAID calculations summed over 19 scattering angles from 0° to 180°. Figure 8 shows another way to look at the sensitivity of observables to the presence or absence of certain resonances. Three different results of MAID are plotted for the differential cross section and the double-polarization observable G for π^+n photoproduction at $W = 1500$ MeV. The MAID full calculation includes the $P_{33}(1232)$, $P_{11}(1440)$, $D_{13}(1520)$, $S_{11}(1535)$, $S_{31}(1620)$, $S_{11}(1650)$, $F_{15}(1680)$, and $D_{33}(1700)$ resonances and is shown as the solid curve. The dashed curve results if one excludes the $P_{11}(1440)$ resonance; the dotted curve excludes the $S_{11}(1535)$ resonance. These different model results have little effect on the differential cross section (upper panel of Figure 8), but are again significantly different for G (lower panel). Despite the simplicity of this comparison — normally the removal of a resonance in any model requires a

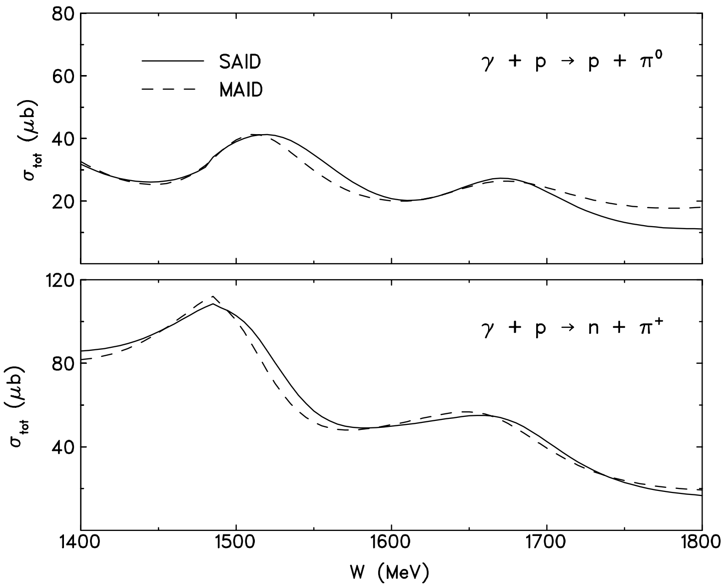

Figure 4: Total cross section for the $\pi^0 p$ and $\pi^+ n$ photoproduction on the proton. The solid and dashed curves show SAID [3] and MAID [4] predictions, respectively.

refitting of the remaining model parameters — it demonstrates the very different sensitivities of cross section and polarization observables.

A final example, using measurements related to the beam-target polarization quantity E, is provided by a recent Mainz study [17]. There, a variation in the $D_{13}(1520)$ photo-decay couplings was suggested in order to explain deviations of the new measurement from predictions of the MAID analysis.

It should be emphasized that a comparison of results from fits to the existing database can give only a hint of what is to be expected. Examples of unexpected results are included in the measurements of $(d\sigma/d\Omega_{1/2} - d\sigma/d\Omega_{3/2})$ [17] and $C_{x,z}$ [13] (See Figure 6). Both experiments produced angular distributions which disagreed with the existing SAID and MAID fits. As is evident from Figure 7 of [17], disagreements with data appeared even in cases where SAID and MAID gave qualitatively similar predictions. As a result, regions of agreement between analyses do not decrease the need for measurements of new quantities. The high sensitivity of single- and double-polarization observables to resonance and interference contributions makes them an indispensable tool for further progress in baryon spectroscopy.

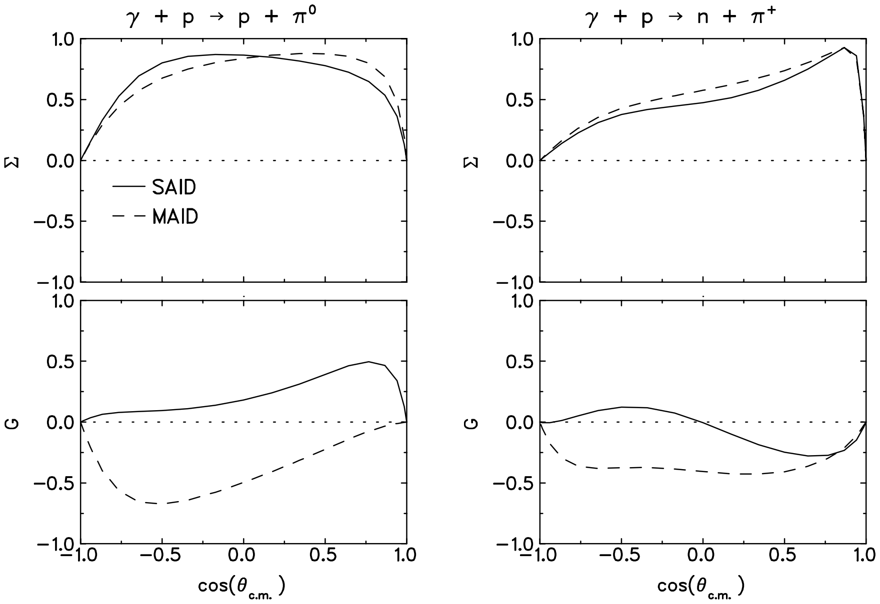

Figure 5: Polarization observables Σ and G in the $p(\gamma, p)\pi^0$ reaction (left panel) and $p(\gamma, \pi^+)n$ reaction (right panel) at $W = 1500$ MeV along with SAID [3] (solid curve) and MAID [4] (dashed curve) results.

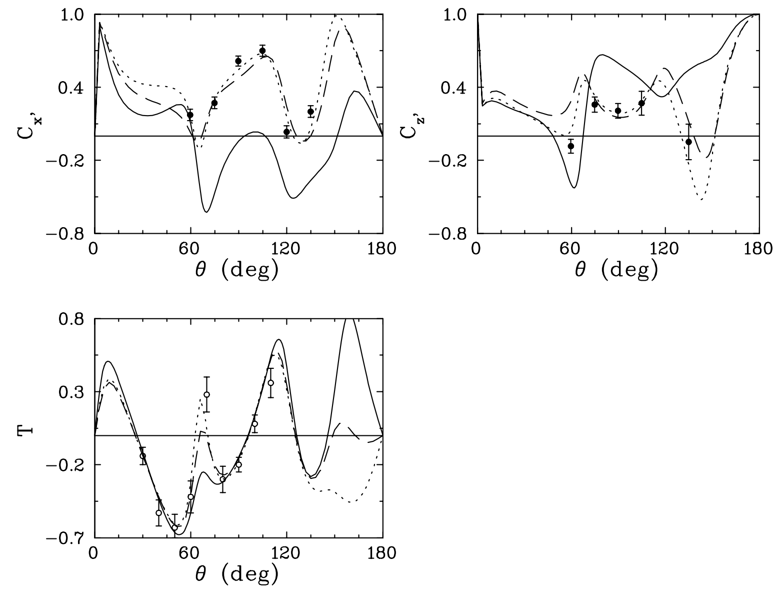

Figure 6: Polarized measurements in neutral pion photoproduction at 1900 MeV; $C_{x'}$ (left top panel), $C_{z'}$ (right top panel), and T (bottom left panel). Solid line gives the SM02 [3] solution. Dashed (dotted) line shows the standard SG02 (forced SC02) solution [14] including the data of Ref. [13] (solid circles). T data (open circles) are from DNPL [15, 16].

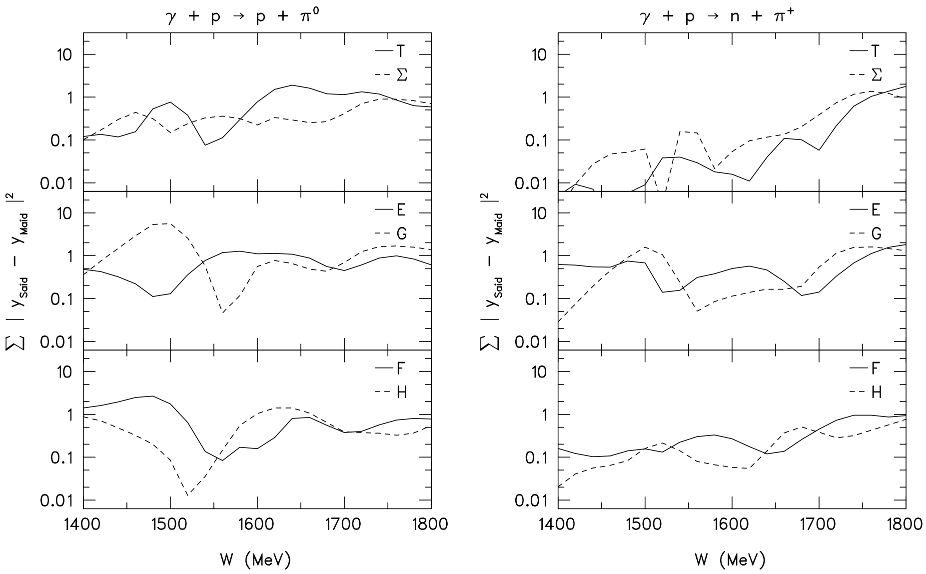

Figure 7: Comparison between SAID and MAID calculations for selected polarization observables in the $p(\gamma,p)\pi^0$ reaction (left panel) and $p(\gamma,\pi^+)n$ reaction (right panel). Plotted is the squared difference between the SAID [3] and MAID [4] results summed over 19 scattering angles from 0° to 180°.

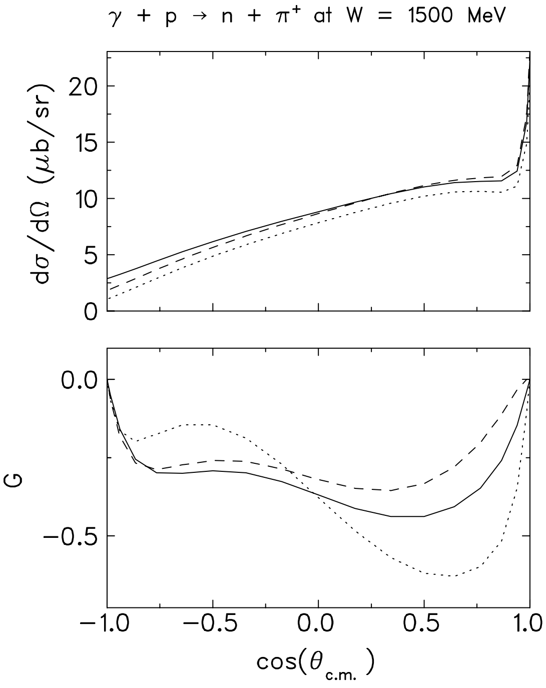

Figure 8: MAID [4] calculations of the differential cross section and double-polarization observable G in the $p(\gamma, \pi^+)n$ reaction at $W = 1500$ MeV; full calculation (solid curve), full calculation with $P_{11}(1440)$ resonance removed (dashed line), full calculation with $S_{11}(1535)$ resonance removed (dotted line).

3 Proposed Measurements

3.1 Kinematics and Proposed Data

We propose to use the Photon Tagging Facility [19] with the CEBAF Large Acceptance Spectrometer CLAS, in Hall B, to perform precision measurements of pion-photoproduction from a polarized proton target in the resonance region. The ability of CLAS to measure over wide ranges in θ_{cm} and ϕ, together with the photon energy information from the tagging facility, provide an ideal environment for these measurements. With circularly polarized photons, we plan to cover the photon-energy range between 0.4 GeV and 2.0 GeV. This provides at low energies a good overlap with the energy range accessible by other laboratories (such as MAMI and GRAAL), and covers the highest energies reliably accessible in partial-wave analyses. With transversely polarized photons, we propose to start at 0.6 GeV; the energy range between 0.4 GeV and 0.6 GeV would require additional settings which we consider not to be justified. An overview of the proposed settings with different beam and target polarizations, along with the accessible observables, is given in Table 4. To facilitate the discussion, we have included setting D, which is not part of this proposal, but a subset of the approved experiment E01-104. A detailed list of the individual settings is given in Table 11 below.

Table 4: Proposed settings. Setting D is a part of experiment E01-104, and not part of this proposal.

Setting	Polarization Beam	Polarization Target	E_γ (GeV)	Observables
A	transverse	transverse	0.6 — 2.0	H, P, T
B	circular	transverse	0.4 — 2.0	F, T
C	transverse	longitudinal	0.6 — 2.0	G
D	circular	longitudinal	0.4 — 2.0	E

The most recent SAID solution (SM02) was used to generate $\pi^0 p$ and $\pi^+ n$ Monte-Carlo (MC) data with the expected statistical and systematic errors. The CLAS acceptance, via GEANT simulations, was then applied. Four different beam/target polarization settings were selected (Table 4). The total number of proposed measurements are listed in Table 3. Figure 9 shows two examples of the proposed data for two observables at $E_\gamma = 1.425$ GeV.

3.2 Utility of Proposed Data

While we have demonstrated that new double-polarization experiments are likely to disagree with present analyses, we can estimate the impact these mea-

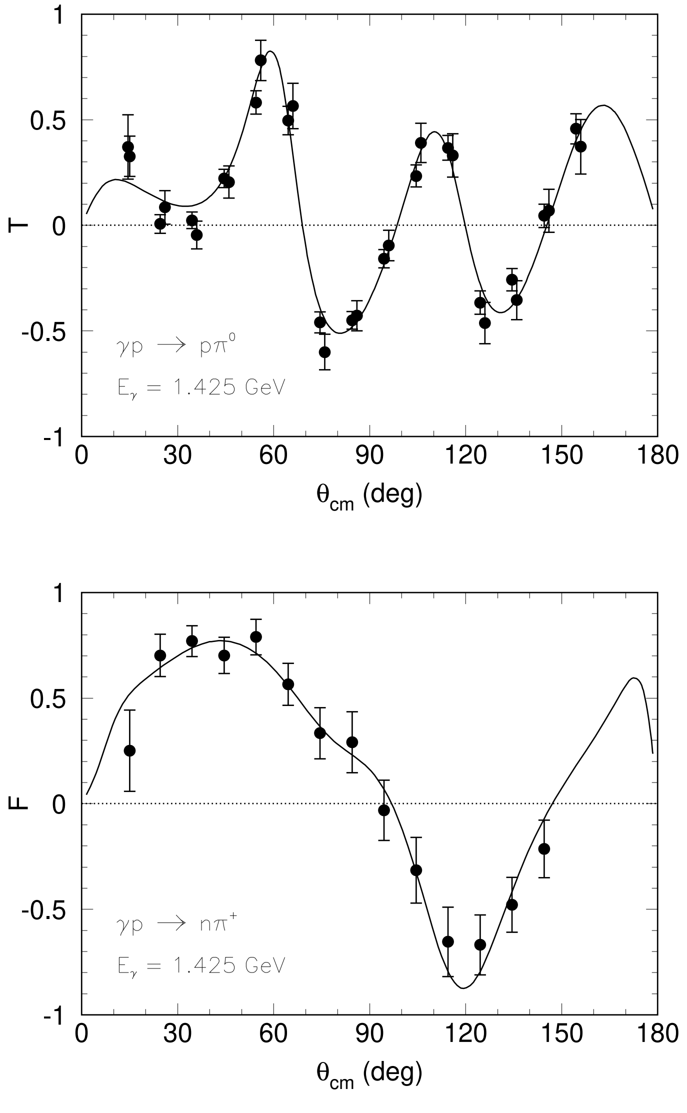

Figure 9: Two examples showing the proposed data for two observables at $E_\gamma =$ 1.425 GeV, for the two different channels. The uncertainties shown are expected statistical errors, only. Only points with absolute uncertainties below 0.20 are shown. Points from different settings are slightly shifted to avoid overlap. The solid curve shows the SAID calculation, which was used to generate the events.

surements will have on fits in the unlikely case that solutions remain stable. This gives, in a sense, the very *least* impact of such measurements. This is accomplished by using the Monte Carlo data described in the previous section. A series of single-energy solutions (SES) have been fitted using settings A, B, C, D, plus a combination including all of them.

To facilitate the comparisons, we have summarized the effect on individual multipoles by computing the ratio of uncertainties with and without the addition of the MC data. A plot of the average ratios is presented in Figure 10. Here we see a particular improvement through the inclusion of sets A or B (transversely polarized target), as compared to C or D (longitudinally polarized target). The greatest effect naturally requires a measurement of all available quantities, but the transversely polarized target provides a great benefit.

We employed both single-energy and energy-dependent solutions over a variety of energy ranges in order to estimate uncertainties. In Figure 11 we present a set of multipoles which shows how the proposed measurements, when added to the available data, can increase the number of SES while reducing uncertainties as well. The proposed measurements, therefore, will lead to a greater sensitivity to missed structures. Figure 12 shows the impact of the proposed data on the SAID single-energy solutions. The new measurements significantly reduce the uncertainties of the observables. The total angular resolution will therefore be greatly improved, enhancing the possibility of determining the number of multipoles that are involved. With this greater understanding of these observables, effects of higher spin resonances can be investigated [20].

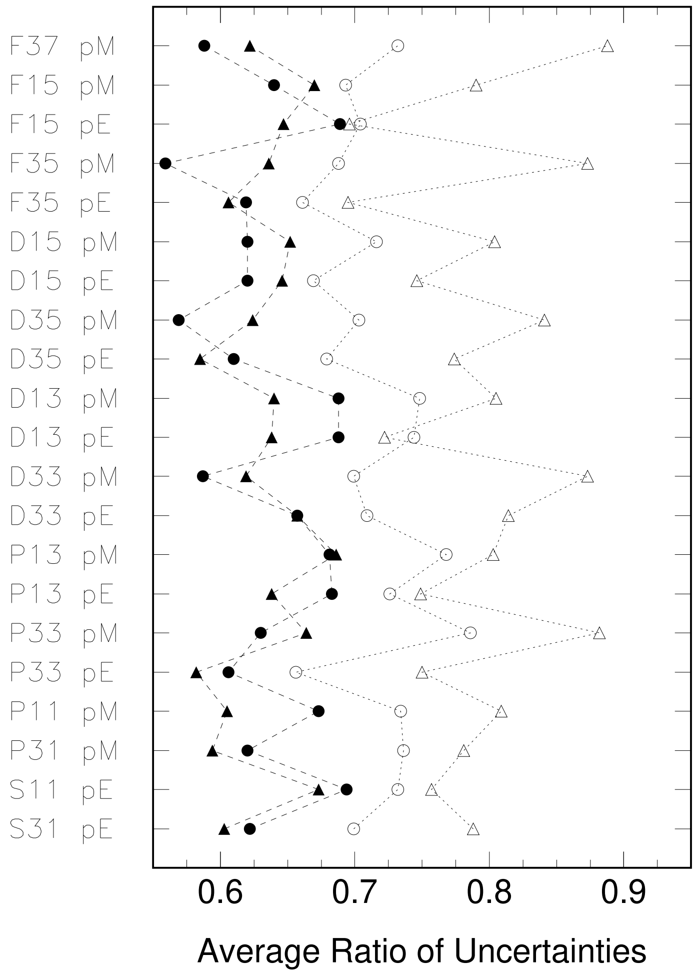

Figure 10: Average ratio of the uncertainties of amplitudes with and without the proposed data individually for the four settings: A (filled circle), B (filled triangle), C (open circle), and D (open triangle).

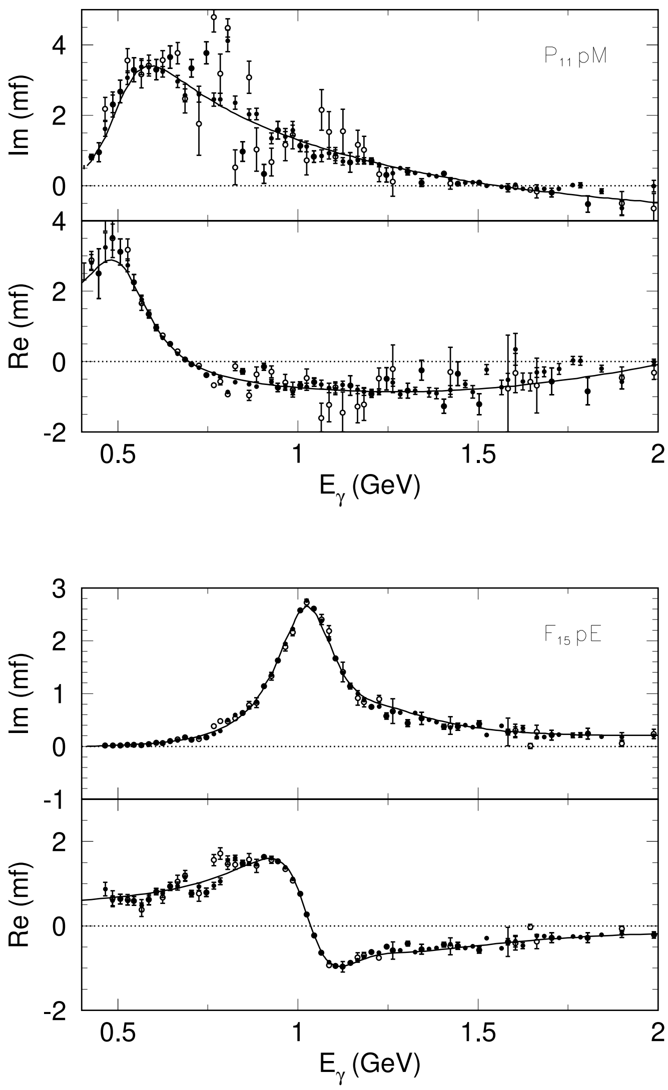

Figure 11: Real and imaginary part of the amplitudes for the multipoles $P_{11}pM$ (upper panel) and $F_{15}pE$ (lower panel); comparison between SAID SM02 (solid curve) along with current SES (open points), and SES after inclusion of the proposed data (filled points).

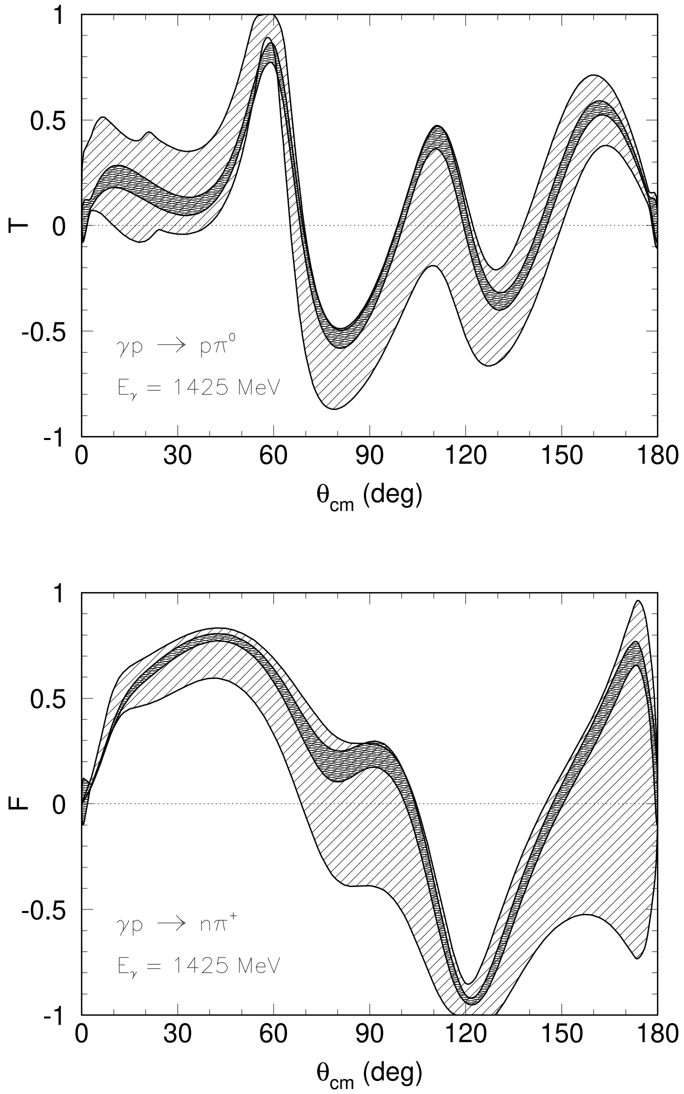

Figure 12: Two examples showing the impact of the proposed data on the SAID single energy solutions (SES). The light hatched band indicates the present uncertainties in the SES, the dark hatched band indicates the uncertainties after including the proposed data into the partial-wave analysis.

4 Apparatus

4.1 Tagged Photon Beam

The tagging facility in Hall B has reliably provided unpolarized, circularly polarized, and linearly polarized tagged-photon beams. Most of the experiments to date have used unpolarized tagged photon beams, at energies between 20% and 95% of the incident electron beam energy E_e.

Circularly polarized photon beams are produced using a beam of longitudinally polarized electrons incident on the bremsstrahlung radiator. The degree of circular polarization of the photon beam depends on the ratio E_γ/E_e, and ranges from 60% to 99% of the incident electron beam polarization P_e for photon energies E_γ between 50% and 95% of the incident electron energy. For this proposal we assume an electron beam polarization of $P_e = 0.70$. With $x = E_\gamma/E_e$, the circular polarization is given by [21]

$$P_\odot = P_e \cdot \frac{4x - x^2}{4 - 4x + 3x^2} \tag{2}$$

Linearly polarized photon beams are produced using coherent bremsstrahlung from a thin diamond radiator. This technique has been successfully employed for the first part of the CLAS-g8 run period. The degree of polarization can reach 80% to 90%, and is a function of the fractional photon beam energy and collimation. With linearly polarized photons, over 80% of the photon flux is confined to a 200-MeV wide energy interval.

4.2 Polarized Target

A polarized target for CLAS completes the requirements for these proposed measurements. A dynamically polarized target was already used for electron beam experiments with the CLAS detector. In this case, to achieve high polarization, the target was located inside a strong and very uniform magnetic field ($B = 5$ T, $\Delta B/B = 10^{-4}$). The high electron polarization is then transferred to the proton via microwave induced transitions. The magnet needed to produce this field occupied a large fraction of the space around the target sample, leaving a relatively small acceptance for outgoing particles. Using a frozen-spin target is the best solution to keep a large acceptance.

The proposed polarized target for use with CLAS would be positioned at the geometrical center of the CLAS in order to maximize acceptance for outgoing reaction products. This requirement sets a number of constraints on the cryostat design and the magnetic field necessary to hold the polarization.

The proposed target cryostat will be a horizontal type with a pipe about 200 cm in length and 40 cm in diameter, which would be inserted to position the target at the center of CLAS, as shown in Figure 13.

Since the CLAS detector is a magnetic spectrometer, its operational characteristics are very sensitive to the additional magnetic field produced by the

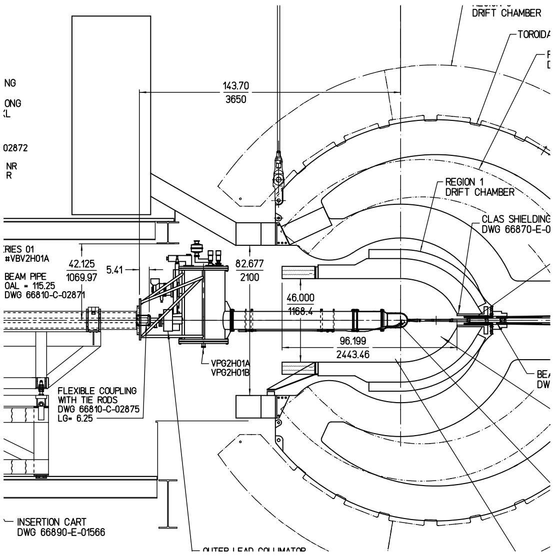

Figure 13: Schematic of proposed polarized target inside the CLAS detector.

target. Since large magnetic fields (typically several Tesla) are required to generate a high degree of polarization in typical target material, such field strengths are too large to successfully operate inside the CLAS detector while permitting good acceptance coverage. To overcome this, the polarized target will be operated in so-called frozen-spin mode. In this case, the target material is polarized outside the CLAS detector in the usual way (magnetic field of 5.0 T and at a temperature of 300 mK – 500 mK). After the maximal polarization is achieved, the cryostat is switched to holding mode, where the microwaves are switched off, and the target temperature is lowered to 50 mK – 70 mK, and the magnetic field is reduced to a holding field of 0.5 T. In this holding mode, the target polarization slowly decreases with a relaxation time of typically several days for the conditions described above. This is sufficiently long for a useful polarized target. Repolarization requires putting the target back into the high field, this procedure takes a few hours.

The target material for the polarized target must meet a number of criteria to create a useful target for photonuclear experiments. It should have a large number of polarizable nuclei, produce high polarization levels, and, for a frozen-spin target, have a relaxation time exceeding 100 hours; sufficiently long to permit the target to be moved into the CLAS detector and data to be acquired with the target.

Several suitable candidates for the target material are compound materials such as alcohols or ammonia. A drawback of using a compound target material is that only the hydrogen component of the target is polarized. For a butanol target, the dilution factor (the fraction of polarizable nucleons) is approximately 13.5%. There already exists many years of experience in constructing and operating such targets.

The JLab target group has started to design and construct a target using butanol for the target material [22]. Such a target would be similar to the polarized target constructed and successfully operated for experiments using the photonuclear facilities in Mainz and Bonn, Germany [23]. Such butanol targets have been constructed with maximum polarizations of 85% – 90%.

The characteristics of the photon beam produced by the Hall B tagged photon facility defines the geometry of the target cell. With a beam spot of diameter up to 12 mm at the target position, the minimum target diameter should be 15 mm. The optimal target length is driven by the (conflicting) demands of count rate (which requires a long target) and cooling requirements (which are easier for a shorter target.) The length has been optimized through simulation of the various photonuclear processes in the target, and was found to be about 50 mm.

Table 5: Target parameters for the Frozen Spin Butanol target.

Chemical structure	C_4H_9OH
Target length	5 cm
Dilution factor	10/74
Density	0.985 g/cm^3
Packing factor	0.62 ± 0.04
Effective density	0.611 g/cm^3
Longitudinal polarization (average)	0.80
Transverse polarization (average)	0.80

4.3 Trigger

The trigger for the proposed experiment requires the detection of at least one charged particle in the CLAS detector; the proton for the $p\pi^0$ reaction channel, and the π^+ for the $n\pi^+$ reaction channel. The trigger condition is consistent with the required trigger setting in experiment E01-104 [24], and the Hyperon Photoproduction experiment E02-112 [25], and allows for sharing of beam time with transversely polarized beam on a transversely polarized target.

5 Running Conditions and Time Estimates

5.1 Event Identification, Reconstruction, Acceptances

The analysis of the reactions $\gamma p \to \pi^0 p$ and $\gamma p \to \pi^+ n$ will be done using the standard particle identification procedure for protons and positive pions detected in CLAS. Undetected particles (π^0 and neutron) will be reconstructed using the missing-mass technique assuming two-body kinematics. This method was developed and has proven successful for the unambiguous selection of reaction channels in the analysis of CLAS-g1 data [6]. Preliminary results of CLAS g1c differential cross section data are shown in Figure 14 along with old data and SAID and MAID predictions. The preliminary CLAS data show reasonable agreement with SAID and MAID results, even though they were not included in either analysis.

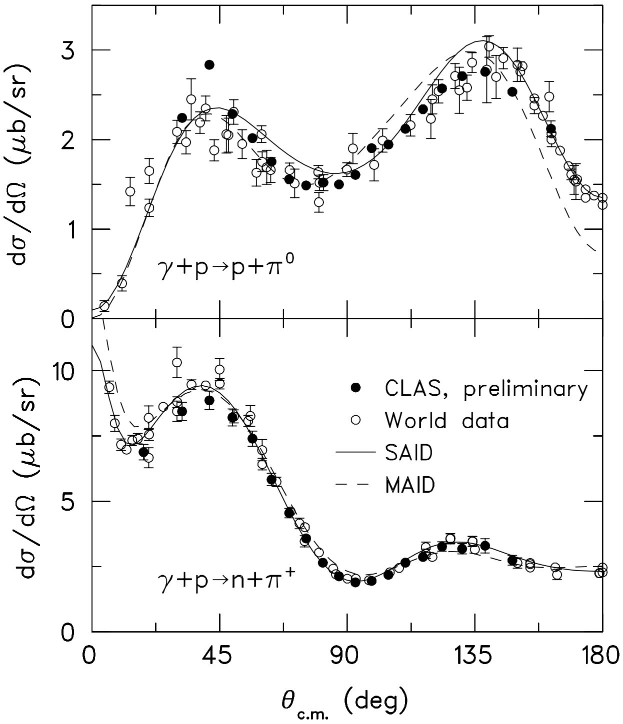

Figure 14: Preliminary differential cross section data at $E_\gamma = 1000$ MeV from the CLAS g1c run group (solid circles) [6]. Analysis by M. Wood for the $p(\gamma, p)\pi^0$ reaction (upper panel), and by R. Schumacher and J. McNabb for the $p(\gamma, \pi^+)n$ reaction (lower panel). These data are compared to other world data (open circles), along with SAID (solid line) and MAID (dashed line) predictions.

The important difference between the proposed experiment and previous photoproduction experiments with CLAS is an extra source of a background associated with the reaction on bound target nucleons.

The dilution factor was estimated for this proposal. Figure 15 shows the missing-mass-squared distributions for the reaction channels under study. The dotted histogram shows the photon-flux-normalized yield for the γp reaction (g1c data), the dashed histogram shows the normalized yield for the γ^4He reaction (g3a data), both integrated over a photon energy range between 0.6 GeV and 1.4 GeV, and over the full CLAS acceptance, requiring the detection of only one charged particle. To estimate the result for the photoreaction on the butanol target (C_4H_9OH), the former distribution was scaled to correspond to the scattering off 10 protons, the latter to the scattering off 64 nucleons. This approach assumes as a good approximation that the nucleon momentum distributions and the per-nucleon photo cross sections for ^{4}He are similar to those of the target nuclei ^{12}C and ^{16}O. The solid histogram shows the sum of both distributions. The dilution factor is then given by the ratio of the proton-to-total yield in the kinematical region of interest, indicated by the dash-dotted line. Based on this approach, our estimate for the dilution factor is $f \approx 0.43$, which is about a factor of 3 improvement on the naive expectation of 10/74.

This unpolarized background constitutes an additional source of the systematic uncertainty. In order to keep it under control, we plan to place an additional carbon target downstream of the main target and collect data from both targets simultaneously.

The acceptance of CLAS for the reactions $\gamma p \to p\pi^0$ and $\gamma p \to n\pi^+$ was obtained by means of a Monte Carlo simulation of the detector. The cross sections were taken from the SAID parametrization, while the detector simulation and event reconstruction utilized the CLAS standard software packages (*gsim*, and *a1c*). The simulation assumes a 5 cm long butanol target, and a main-torus current of +1920 A. The torus current was chosen to be compatible with the experiments E01-104 and E02-112. The results are shown in Figure 16. Other target lengths and torus currents lead to very similar results. The product of the acceptance and efficiency is on average between 0.5 and 0.7. It is slightly energy dependent, and the angular range with an appreciable acceptance is limited to $\theta_{cm} = 20^\circ - 160^\circ$. The count-rate estimates make use of the full energy and angle coverage.

5.2 Projected Results

5.2.1 Count Rate Estimates

The expected count rate for pion photoproduction events produced off free (polarized) protons in a specific kinematic bin is given by

$$\dot{N}_{\text{pol}} = \sigma_P \cdot \dot{\Phi} \cdot \frac{\rho_{\text{tgt}} x_{\text{tgt}} N_A}{A_{\text{Butanol}}} \cdot 10, \tag{3}$$

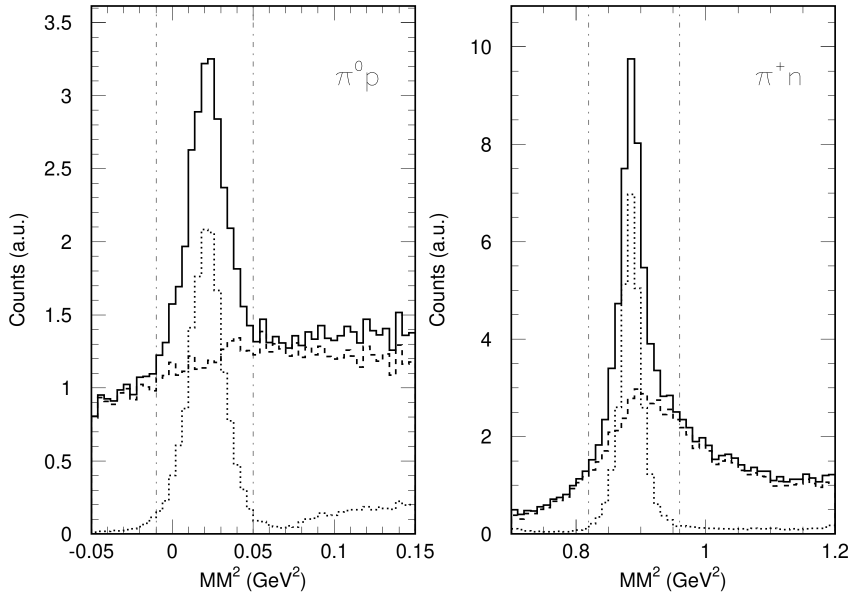

Figure 15: Normalized missing-mass-square distributions to estimate the value of the dilution factor; scattering events from hydrogen (dotted histogram), unpolarized bound nucleons (dashed), and their total (solid). The dot-dashed line indicates the kinematical region of interest.

where σ_P is the integrated cross section for that bin, $\dot{\Phi}$ is the photon flux at the target, $\rho_{\rm tgt}$, $x_{\rm tgt}$, and $A_{\rm Butanol}$ are respectively, the density, length, and molar mass of the target, and N_A is Avogadro's number. The factor of 10 accounts for the number of ^{1}H atoms in the Butanol molecule. As for the acceptance studies, the integrated cross sections for the two different pion-photoproduction channels were obtained by means of a Monte Carlo simulation of CLAS using SAID polarized cross sections, thus it includes the acceptance and efficiency of the CLAS detector.

We have chosen a fine binning in the relevant kinematical variables; for the photon energy $\Delta E_\gamma = 50$ MeV, and for pion center-of-mass angle $\Delta\theta_{\rm cm} = 10°$.

The total luminosity is restricted by maximum rates of the tagger, the data acquisition system, and accidental background. To ensure that the experimental rates are kept within those limits, we have adjusted the proposed photon flux assuming the parameters of Table 6 and the total cross section per nucleon shown in Figure 17. The total per-nucleon photo cross section on lead

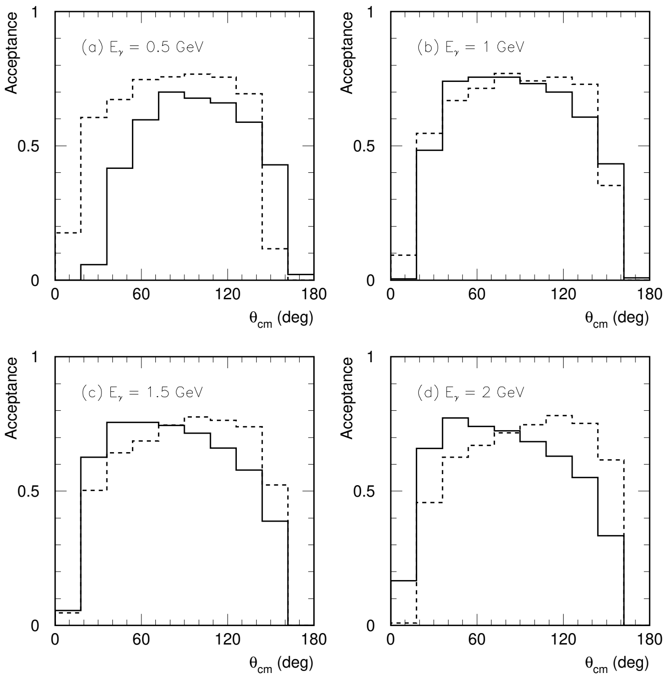

Figure 16: Pion angle, θ_{cm}, dependence of the product of the acceptance and efficiency of CLAS at different photon energies and for the reactions $\gamma p \rightarrow p\pi^0$ (solid histogram) and $\gamma p \rightarrow n\pi^+$ (dashed histogram).

is a good approximation of the per-nucleon cross sections of the butanol target materials carbon and oxygen. The mean tagging efficiency was estimated by calculating the transmitted fraction through the collimator using tabulated bremsstrahlung angular distribution calculations [26]. A collimator at a distance of 5.8 m and with a diameter of 2.6 mm for circularly polarized photons was assumed. Settings A and C with linearly polarized photons will run with a collimator diameter of 2.0 mm.

5.2.2 Polarization Predictions

With the target polarization in the reaction frame (see Figure 18), given by

$$\begin{aligned} P_X &= P_{XY}^{\text{lab}} \cdot \cos(\beta - \phi) && (4) \\ P_Y &= P_{XY}^{\text{lab}} \cdot \sin(\beta - \phi) && (5) \\ P_Z &= P_Z^{\text{lab}}, && (6) \end{aligned}$$

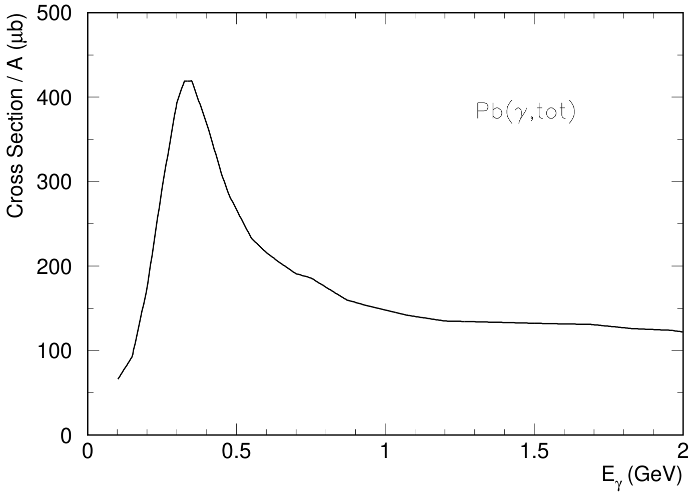

Figure 17: Total γ+Pb cross section per nucleon. Parametrization courtesy of I. Pshenichnov [27].

Table 6: Parameters for rate estimates.

Maximum tagger rate	30	MHz
Maximum tagger rate per T-counter	4-5	MHz
Maximum CLAS DAQ rate	3.5	kHz
Mean tagging efficiency (at $E_e = 1.6$ GeV)	0.18	
Mean tagging efficiency (at $E_e = 2.2$ GeV)	0.40	
Coincidence time window	15	ns
CLAS acceptance for a hadronic event	0.70	

and the angle of the transverse beam-polarization direction with respect to the reaction plane, $\varphi = \alpha - \phi$, the polarized cross section, Eq. (1), can be rewritten as:

$$\begin{aligned} \frac{1}{\sigma_0} \cdot \frac{d\sigma}{d\Omega} &= 1 \\ &\quad -P_\odot P_Z^{\rm lab} \cdot E \\ &\quad +P_\odot P_{XY}^{\rm lab} \cdot \cos(\beta - \phi) \cdot F \end{aligned}$$

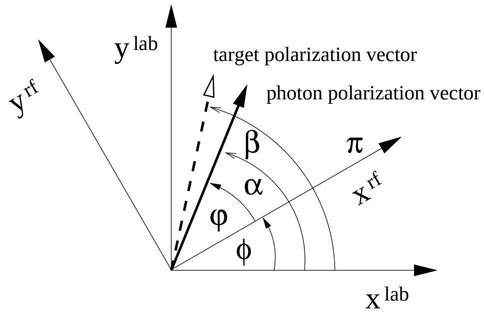

Figure 18: Relative orientations of reference frames and beam/target polarizations. The z-direction (beam axis) of the laboratory (lab) and reaction (rf) frames coincide. The x^{rf}-direction is defined by the pion momentum.

$$\begin{aligned}
&+P_{XY}^{\mathrm{lab}} \cdot \sin(\beta - \phi) \cdot T \\
&-P_T \cdot \cos 2(\alpha - \phi) \cdot \Sigma \\
&+P_T P_Z^{\mathrm{lab}} \cdot \sin 2(\alpha - \phi) \cdot G \\
&-P_T P_{XY}^{\mathrm{lab}} \cdot \cos(\beta - \phi) \sin 2(\alpha - \phi) \cdot H \\
&-P_T P_{XY}^{\mathrm{lab}} \cdot \sin(\beta - \phi) \cos 2(\alpha - \phi) \cdot P \ . \qquad (7)
\end{aligned}$$

The experimentally observed angular distribution, $A_{\mathrm{exp}}(\phi)$, is the weighted sum of the distributions coming from polarized protons and other, unpolarized, target materials:

$$A_{\mathrm{exp}} = \frac{A_{\mathrm{pol}} N_{\mathrm{pol}} + A_{\mathrm{unpol}} N_{\mathrm{unpol}}}{N_{\mathrm{pol}} + N_{\mathrm{unpol}}} \qquad (8)$$

The target nuclei ^{12}C and ^{16}O have spin 0, and are unpolarized; thus for all target and beam/target polarization observables the asymmetry A_{unpol} vanishes. Knowing the dilution factor $f = N_{\mathrm{pol}}/(N_{\mathrm{pol}} + N_{\mathrm{unpol}})$, the asymmetry of interest can be extracted as

$$A_{\mathrm{pol}} = \frac{1}{f} A_{\mathrm{exp}} \ . \qquad (9)$$

The polarization observables of interest can be extracted by means of a Fourier analysis of the experimental azimuthal angular distribution. The estimator and the standard uncertainty is given by

$$O = \frac{1}{f_{\mathrm{eff}}} \cdot \frac{\sum w_i}{\sum w_i^2} \quad \text{and} \quad u(O) = \frac{1}{f_{\mathrm{eff}}} \sqrt{\frac{\kappa}{N}} \ , \qquad (10)$$

where the sums are running over all events in the considered kinematical bin and O stands for E, T, Σ, G, F, H, or P. The standard uncertainty depends on the total number of events in that bin, $N = N_{\mathrm{pol}}/f$, and a scale factor κ. The factor κ accounts for differences in the way observables enter the cross section Eq. (7); for no angular dependence ($\kappa = 1$), as a single Fourier coefficient ($\kappa = 2$), or as a linear combination of two Fourier coefficients ($\kappa = 4$). The weights w_i, effective dilution factors f_{eff}, and scale factors are different for each observable, and given in Table 7.

Table 7: Extraction of target and beam/target polarization observables from azimuthal angular distributions.

Observable	Weight w_i	f_{eff}	κ
E	$-h_i$	$P_{\odot} P_Z^{\text{lab}} f$	1
T	$\sin(\beta_i - \phi_i)$	$P_{XY}^{\text{lab}} f$	2
Σ	$-\cos 2(\alpha_i - \phi_i)$	$P_T P_{XY}^{\text{lab}} f$	2
G	$\sin 2(\alpha_i - \phi_i)$	$P_T P_Z^{\text{lab}} f$	2
F	$h_i \cos(\beta_i - \phi_i)$	$P_{\odot} P_{XY}^{\text{lab}} f$	2
H	$-\cos(\beta_i - \phi_i) \sin 2(\alpha_i - \phi_i)$	$P_T P_{XY}^{\text{lab}} f$	4
P	$-\sin(\beta_i - \phi_i) \cos 2(\alpha_i - \phi_i)$	$P_T P_{XY}^{\text{lab}} f$	4

Since all three polarization observables T, H, and P have Fourier components in the first order of $\sin\phi$ or $\cos\phi$, it is mandatory to take data with beam and/or target polarizations flipped to disentangle these observables. The approach to extract the polarization observables as weighted sums was tested with the Monte Carlo data. Figure 19 gives an example for observables G and H for the $\pi^0 p$ channel.

A summary of the amount and anticipated statistical uncertainties of the proposed data is given in Tables 8 and 9.

5.2.3 Systematic Uncertainties

The main systematic uncertainties are due to uncertainties in the beam and target polarizations, the dilution factor, and instrumental asymmetries in the angular distributions. The systematic uncertainties from instrumental asymmetries can be minimized by flipping the helicity of the target nucleons and incident photons. The target polarization should be changed with every re-polarization. An estimate of the contributing uncertainties is given in Table 10, see [25]. For the longitudinally polarized target an occasional measurement of the polarization can be performed since the holding field should be sufficiently homogeneous. NMR measurements should be done roughly every hour in addition to the measurements at the beginning and end of cycles. For the transversely polarized target, a continuous measurement of the target polarization may be more difficult and may require additional material to get a homogeneity similar to the longitudinally polarized target. Thus NMR measurements will be performed at the beginning and end of cycles after the spin rotation. The dilution factor

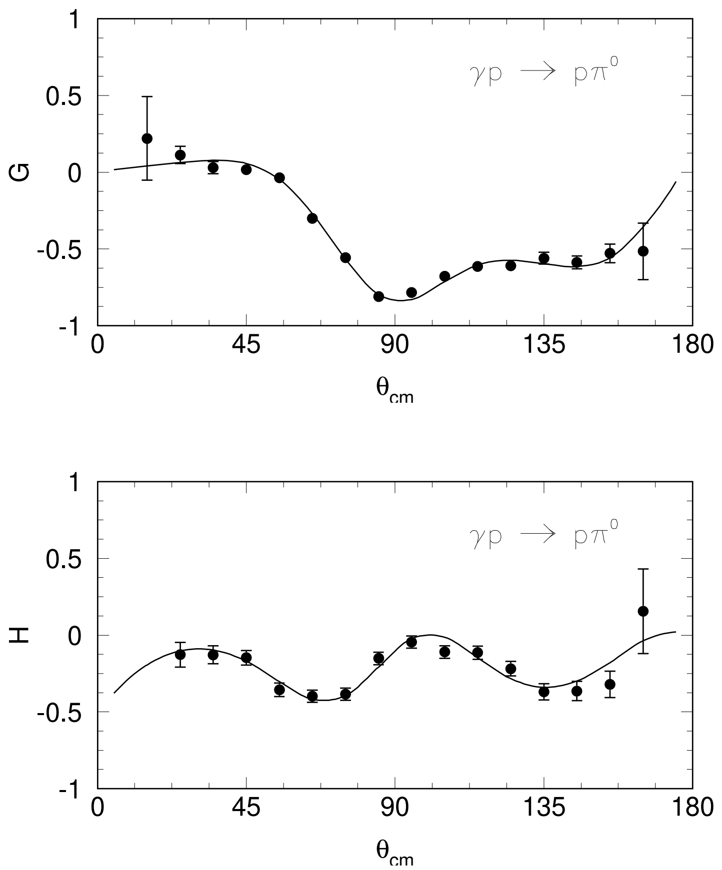

Figure 19: Extraction of the polarization observable G (upper panel) and H (lower panel) from Monte Carlo data at $E_\gamma = 1000$ MeV. The solid curve is the underlying SAID parametrization on which the Monte Carlo event generator was based.

will be determined from the data taken on a thin carbon target placed downstream of the frozen spin target and data from special runs with the unpolarized butanol target. The anticipated uncertainties on the observables are given in Table 10 as well.

Table 8: Mean uncertainty ($\bar{u}$) and number of data points (n) for the proposed $\gamma + p \to p + \pi^0$ data. Only data with $u < 0.20$ are included in this table.

Set:	A		A		A & B		B		C	
E_γ	H		P		T		F		G	
(GeV)	$\bar{u}_H$	n_H	$\bar{u}_P$	n_P	$\bar{u}_T$	n_T	$\bar{u}_F$	n_F	$\bar{u}_G$	n_G
0.425	—	—	—	—	0.03	14	0.07	12	—	—
0.475	—	—	—	—	0.02	13	0.07	12	—	—
0.525	—	—	—	—	0.03	13	0.08	12	—	—
0.575	—	—	—	—	0.03	13	0.09	12	—	—
0.625	0.08	13	0.08	13	0.05	27	0.09	12	0.08	13
0.675	0.08	13	0.08	13	0.05	28	0.08	12	0.08	13
0.725	0.08	14	0.08	14	0.05	29	0.08	13	0.08	14
0.775	0.05	14	0.05	14	0.04	30	0.08	14	0.05	14
0.825	0.06	14	0.06	14	0.04	29	0.08	14	0.06	14
0.875	0.07	14	0.07	14	0.05	29	0.09	14	0.07	14
0.925	0.09	14	0.09	14	0.05	28	0.09	14	0.09	14
0.975	0.08	14	0.08	14	0.05	28	0.08	14	0.08	14
1.025	0.08	14	0.08	14	0.05	29	0.07	14	0.08	14
1.075	0.06	14	0.06	14	0.04	28	0.08	14	0.06	14
1.125	0.07	14	0.07	14	0.05	28	0.09	14	0.07	14
1.175	0.09	14	0.09	14	0.06	29	0.11	14	0.09	14
1.225	0.09	15	0.09	15	0.07	30	0.11	14	0.09	15
1.275	0.08	14	0.08	14	0.07	29	0.11	14	0.08	14
1.325	0.09	15	0.09	15	0.07	30	0.11	14	0.09	15
1.375	0.09	15	0.09	15	0.07	30	0.11	14	0.09	15
1.425	0.09	15	0.09	15	0.07	30	0.12	15	0.09	15
1.475	0.10	15	0.10	15	0.06	44	0.10	29	0.10	15
1.525	0.11	15	0.11	15	0.06	30	0.08	15	0.11	15
1.575	0.11	15	0.11	15	0.06	30	0.09	15	0.11	15
1.625	0.12	15	0.12	15	0.07	30	0.10	15	0.12	15
1.675	0.10	15	0.10	15	0.06	30	0.10	15	0.10	15
1.725	0.10	14	0.10	14	0.06	30	0.10	14	0.10	14
1.775	0.11	14	0.11	14	0.07	30	0.10	14	0.11	14
1.825	0.12	14	0.12	14	0.07	30	0.11	14	0.12	14
1.875	0.11	13	0.11	13	0.07	29	0.10	13	0.11	13
1.925	0.12	13	0.12	13	0.08	29	0.11	13	0.12	13
1.975	0.12	13	0.12	13	0.07	28	0.11	13	0.12	13
Total		396		396		884		452		396

Table 9: Mean uncertainty ($\bar{u}$) and number of data points (n) for the proposed $\gamma + p \to n + \pi^+$ data. Only data with $u < 0.20$ are included in this table.

Set:	A		A		A & B		B		C	
E_γ	H		P		T		F		G	
(GeV)	$\bar{u}_H$	n_H	$\bar{u}_P$	n_P	$\bar{u}_T$	n_T	$\bar{u}_F$	n_F	$\bar{u}_G$	n_G
0.425	—	—	—	—	0.01	14	0.06	14	—	—
0.475	—	—	—	—	0.01	14	0.06	14	—	—
0.525	—	—	—	—	0.02	14	0.06	14	—	—
0.575	—	—	—	—	0.02	14	0.06	14	—	—
0.625	0.05	14	0.05	14	0.03	30	0.05	14	0.05	14
0.675	0.05	15	0.05	15	0.03	30	0.05	14	0.05	15
0.725	0.05	15	0.05	15	0.03	30	0.05	14	0.05	15
0.775	0.04	15	0.04	15	0.03	30	0.06	15	0.04	15
0.825	0.05	15	0.05	15	0.03	30	0.06	15	0.05	15
0.875	0.05	15	0.05	15	0.03	30	0.07	15	0.05	15
0.925	0.06	15	0.06	15	0.04	30	0.07	15	0.07	15
0.975	0.06	15	0.06	15	0.04	30	0.06	15	0.06	15
1.025	0.06	15	0.06	15	0.04	30	0.07	15	0.06	15
1.075	0.05	15	0.05	15	0.04	30	0.07	15	0.05	15
1.125	0.06	15	0.06	15	0.04	30	0.08	15	0.06	15
1.175	0.08	15	0.08	15	0.05	30	0.09	15	0.08	15
1.225	0.08	15	0.08	15	0.06	30	0.10	15	0.07	15
1.275	0.08	15	0.08	15	0.06	30	0.11	15	0.08	15
1.325	0.09	15	0.09	15	0.06	29	0.11	14	0.08	15
1.375	0.08	15	0.08	15	0.06	30	0.11	15	0.09	15
1.425	0.09	15	0.09	15	0.07	30	0.11	14	0.09	15
1.475	0.09	14	0.09	14	0.06	45	0.10	30	0.09	14
1.525	0.10	15	0.10	15	0.05	30	0.08	15	0.10	15
1.575	0.10	14	0.10	14	0.06	30	0.08	15	0.11	14
1.625	0.11	14	0.11	14	0.06	29	0.08	15	0.11	13
1.675	0.09	15	0.09	15	0.05	30	0.09	15	0.09	15
1.725	0.09	15	0.09	15	0.06	30	0.09	15	0.09	15
1.775	0.10	14	0.10	14	0.06	30	0.10	14	0.10	14
1.825	0.11	14	0.11	14	0.07	30	0.10	14	0.11	14
1.875	0.12	14	0.12	14	0.07	30	0.11	14	0.11	13
1.925	0.11	12	0.11	12	0.07	30	0.11	14	0.11	13
1.975	0.12	12	0.12	12	0.08	30	0.11	14	0.12	12
Total		407		407		909		481		406

Table 10: Systematic uncertainties. Numbers are taken from [25].

Quantity		Uncertainty
Transverse beam polarization	P_T	5% – 6%
Circular beam polarization	$P_\odot$	4%
Transverse target polarization	P_{XY}	3% – 4%
Longitudinal target polarization	P_Z	3% – 4%
Dilution factor	f	3% – 4%
Observable	T	4% – 6%
	F	6% – 7%
	G, H, P	7% – 8%

6 Summary and Beam Time Request

We propose to use the CLAS and the photon tagging facility in Hall B at Jefferson Lab, together with a frozen-spin polarized target, to perform high-precision measurements of the observables T, P, G, F, and H in single pion photoproduction for W in the range between 1300 MeV and 2150 MeV and covering $\cos(\theta_{cm})$ from -0.9 to 0.9, utilizing the full angular acceptance of CLAS. These measurements will provide a high-precision data set, with small statistical uncertainties and well-understood systematic uncertainties, which will be used in partial-wave analyses of photoproduction data to improve the quality of the global fits and to reduce the uncertainties due to model dependence when extracting resonance parameters from the data.

This proposed experimental program is a natural continuation of the measurements already made on pion photoproduction from the nucleon, performed with CLAS in experiment E94–103 [6]. In addition, a number of other proposals to study photoproduction of other mesons $(K, \eta, \eta', \rho, \omega, \ldots)$ using a spin-polarized target are being prepared; see, *e.g.,* [28]. The experimental requirements for these other measurements are similar to those for the presently proposed measurements, permitting the data to be taken concurrently for all the meson photoproduction experiments (as already demonstrated by the successful g1 run). The Hyperon E02–112 [25] experiment includes a setting which requires a linearly polarized beam incident on a transversely polarized target; this corresponds to the higher-energy part ($E_\gamma > 1.15$ GeV) of setting A of this proposal. Experiment E02-112 has been approved for 20 days of beam time. Assuming that a sufficient fraction of these days are being spent on that setting, it is sufficient to request four additional days for the lower energy part of setting A.

Overhead time is dedicated to beam energy changes, beam- and target-polarization changes, and repolarizations, as well as polarization measurements. The major impact comes from reversing the target polarization (estimated to be 6 h) and the multiple changes in the orientation of the direction of the linearly polarized photon beam (0.5 h). Beam energy changes can be scheduled in parallel with target repolarizations.

In total we request 32 days for the proposed measurements, including 23 days with beam on target and 9 days of overhead. Some fraction of the overhead time can be scheduled to coincide with accelerator maintenence or development time. A summary of the beam time request is given in Table 12.

Table 11: Proposed kinematics in the settings (Set.) A, B, and C; given are the type of photon (Beam), and target (Tgt.) polarization, collimator diameter (d_c), proposed running time, incident electron beam energy, covered photon energy range, assumed photon flux at target $\dot{\Phi}$ within the used tagger range (Tgr.).

Set.	#	Beam	Tgt	d_c (mm)	Time (h)	E_e (GeV)	E_γ (GeV)		$\dot{\Phi}$ (MHz)	Tgr. (MeV)
A	1	lin	trans	2.0	16	2.0	0.600	0.750	5.0	200
A	2	lin	trans	2.0	32	2.0	0.750	0.900	5.0	200
A	3	lin	trans	2.0	16	3.0	0.900	1.050	5.0	200
A	4	lin	trans	2.0	32	3.0	1.050	1.200	5.0	200
A	5	lin	trans	2.0	32	4.0	1.200	1.350	5.0	200
A	6	lin	trans	2.0	32	4.0	1.350	1.500	5.0	200
A	7	lin	trans	2.0	32	4.0	1.500	1.650	5.0	200
A	8	lin	trans	2.0	64	4.0	1.650	1.800	5.0	200
A	9	lin	trans	2.0	64	4.0	1.800	1.950	5.0	200
A	10	lin	trans	2.0	64	4.0	1.950	2.000	5.0	200
B	11	circ	trans	2.6	110	1.6	0.400	1.500	6.6	full
B	12	circ	trans	2.6	145	2.2	1.450	2.000	4.9	part
C	13	lin	long	2.0	8	2.0	0.600	0.750	5.0	200
C	14	lin	long	2.0	16	2.0	0.750	0.900	5.0	200
C	15	lin	long	2.0	8	3.0	0.900	1.050	5.0	200
C	16	lin	long	2.0	16	3.0	1.050	1.200	5.0	200
C	17	lin	long	2.0	16	4.0	1.200	1.350	5.0	200
C	18	lin	long	2.0	16	4.0	1.350	1.500	5.0	200
C	19	lin	long	2.0	16	4.0	1.500	1.650	5.0	200
C	20	lin	long	2.0	32	4.0	1.650	1.800	5.0	200
C	21	lin	long	2.0	32	4.0	1.800	1.950	5.0	200
C	22	lin	long	2.0	32	4.0	1.950	2.000	5.0	200

Table 12: Summary of beam time request including overhead time.

Set.	In Parallel	Purpose	Time (days)	
			Required	This Request
A	E02-112	Production	16.0	4.0
		Tgt. pol. change (10×)	2.5	2.5
		Beam pol. change (80×)	1.7	1.7
B	—	Production	10.6	10.6
		Tgt. pol. change (3×)	0.8	0.8
C	—	Production	8.0	8.0
		Tgt. pol. change (10×)	2.5	2.5
		Beam pol. change (80×)	1.7	1.7
All		Production	34.6	22.6
		Overhead	9.2	9.2
		Total	43.8	31.8

References

[1] B. M. K. Nefkens, in *Proceedings of the GW/JLab Workshop on N^* Physics, The George Washington University–Virginia Campus, 1997*, edited by H. Haberzettl, C. Bennhold, and W. J. Briscoe [πN Newsletter, **14**, 150 (1998)]; E. Klempt, Eprint nucl-ex/0203002; T. D. Cohen and L. Y. Glozman, Int. J. Mod. Phys. A **17**, 1327 (2002).

[2] S. Capstick and W. Roberts, Prog. Part. Nucl. Phys. (Suppl. 2) **45**, 241 (2000).

[3] R. A. Arndt, W. J. Briscoe, I. I. Strakovsky, and R. L. Workman, Phys. Rev. C **66**, 055213 (2002).

[4] D. Drechsel *et al.*, Nucl. Phys. **A645**, 145 (1999).

[5] R. A. Arndt, I. I. Strakovsky, R. L. Workman, and M. M. Pavan, Phys. Rev. C **52**, 2120 (1995); R. A. Arndt, M. M. Pavan, I. I. Strakovsky, and R. L. Workman, to be submitted to Phys. Rev. C.

[6] Jefferson Lab experiment E94–103: *The Photoproduction of Pions*, W. J. Briscoe, J. Ficenec, and D. Jenkins, spokespersons.

[7] C. Bennhold *et al.*, in *NStar2001: Proceedings of the Workshop on the Physics of Excited Nucleons*, Mainz, Germany , March 7-10, 2001, edited by D. Drechsel and L. Tiator, p. 64 (World Scientific, 2001).

[8] F. X. Lee, S. J. Dong, T. Draper, I. Horvath, K. F. Liu, N. Mathur, and J.B. Zhang, hep-lat/0208070.

[9] S. Capstick and P.R. Page, Phys. Rev. C **66**, 065204 (2002).

[10] I. S. Barker, A. Donnachie, and J. K. Storrow, Nucl. Phys. **B75**, 347 (1975).

[11] W. T. Chiang and F. Tabakin, Phys. Rev. C **55**, 2054 (1997).

[12] O. Bartalini *et al.*, Phys. Lett. **B544**, 113 (2002).

[13] K. Wijesooriya *et al.* Phys. Rev. C **66**, 034614 (2002).

[14] R. A. Arndt, I. I. Strakovsky, and R. L. Workman, Phys. Rev. C **67**, 048201 (2003).

[15] I. M. Barbour, R. L. Crawford, and N. H. Parsons, Nucl. Phys. **B141**, 253 (1978); P. J. Bussey *et al.* Nucl. Phys. **B154**, 492 (1979).

[16] P. J. Bussey *et al.* Nucl. Phys. **B159**, 383 (1979); P. S. L. Booth, DNPL Annual Report, 1977.

[17] J. Ahrens *et al.* Phys. Rev. Lett. **88**, 232002 (2002).

[18] For more information about the physics goals of the collaboration, see http://www.jlab.org/~dgr/lhpc.

[19] D. I. Sober *et al.* Nucl. Instr. Meth. A **440**, 263 (2000).

[20] B. Saghai and F. Tabakin, Phys. Rev. C **53**, 66 (1996). See also G. Keaton and R. Workman, Phys. Rev. C **53**, 1434 (1996).

[21] H. Olsen and L. C. Maximon, Phys. Rev. **114**, 887 (1959).

[22] B. Mecking, http://clasweb.jlab.org/frost .

[23] Ch. Bradtke, *et al.* Nucl. Instr. Meth. A **436**, 430 (1999).

[24] Jefferson Lab experiment E01–104: *Helicity Structure of Pion Photoproduction*, update of E91–015, D. I. Sober, M. Khandaker, and D. G. Crabb, spokespersons.

[25] Jefferson Lab experiment E02–112: *Search for Missing Nucleon Resonances in the Photoproduction of Hyperons Using a Polarized Photon Beam and a Polarized Target*, F. J. Klein, P. Eugenio, and L. Todor, spokespersons.

[26] D. I. Sober, computer code `tageff` and private communication, 2003.

[27] I. Pshenichnov, private communication, 2003.

[28] Jefferson Lab Letter of Intent LOI-02-104: *Measurement of Polarization Observables in η-photoproduction with CLAS*, E. Pasyuk, spokesperson.